ARTICLE OPEN

Check for updates

Optically induced nuclear spin–spin couplings in GaAs manifested by spin echo decays under optical pumping

Atsushi Goto[1]✉, Kenjiro Hashi[1], Shinobu Ohki[1] and Tadashi Shimizu[1]

Optically induced nuclear spin–spin coupling in semiconductors is expected to serve for gate operations in nuclear-magnetic-resonance (NMR) quantum computations. However, not much is known about its characteristics. In this study, we investigate optically induced couplings in GaAs via double-resonance spin-echo decay experiments under optical pumping. The squared echo decay rate $(1/T_2)^2$ of ^{71}Ga measured under various light powers revealed that optically induced couplings increase with increasing light power, and the sign of heteronuclear couplings between Ga–As pairs is opposite to that of dipolar couplings, which cancel each other out. Under higher light power, the optically induced "controllable" coupling is expected to eventually surpass the "uncontrollable" nuclear dipolar coupling, becoming dominant, which is preferable for the gate operation in NMR quantum computation.

npj Quantum Information (2022)8:59 ; https://doi.org/10.1038/s41534-022-00571-x

INTRODUCTION

Nuclear spin–spin coupling (interaction) is a fundamental property in NMR measurements, and it provides crucial information regarding the properties of electronic systems in solids. In metals, for example, the couplings are mediated by spatially modulated electron spins called Ruderman–Kittel interactions[1]. The spatial modulation reflects the topology of the Fermi surface and is manifested as a broadening of the NMR spectrum. Another example can be found in ferro/antiferromagnets, where the Suhl–Nakamura interaction is mediated by virtual magnons[2,3]. The electronic states related to the spin–spin couplings are generalized as dynamic spin susceptibility $\chi(q,\omega)$, with q and ω being the momentum and energy of the magnetic excitation, respectively. This relation has been used to investigate the properties of strongly correlated electron systems. The coupling manifests itself as the transverse relaxation rate $(1/T_2)$, reflecting the real part of the generalized spin susceptibility at nearly zero energy, i.e., $\sum_q \chi(q,\omega\sim 0)$[4–6].

The relationship between the nuclear spin–spin coupling and electronic states can be used in the opposite way: the manipulation of nuclear spin–spin coupling through the modification of electronic states. This mechanism can be used to manipulate nuclear spin states; for example, this type of coupling can be used to control gating in NMR quantum computations[7,8]. In a previous paper, we reported nuclear spin–spin coupling in the compound semiconductor GaAs, observed only under light illumination with the photon energy corresponding to the band gap; this implied a switchable coupling through light illumination[9]. The coupling was manifested in the cross-polarization between ^{71}Ga and ^{75}As nuclear magnetizations enhanced by optical pumping under light illumination. The ^{71}Ga magnetization showed oscillatory behavior as a function of the contact time, and the phase of the oscillation changed systematically depending on the power of the illuminated light. This observation was ascribed to the systematic extension of the reach of the coupling.

The results suggested that the coupling was mediated by photoexcited electrons under light illumination. Nevertheless, because illustrating this phenomenon is complicated through the cross-polarization process, it is preferable to use more direct approaches to analyze the optically induced couplings quantitatively. In particular, it is important to understand the competition between the optically induced couplings and the nuclear dipolar couplings. Since the former is controllable (switchable) while the latter is uncontrollable, ensuring that the strength and reach of the former surpasses those of the latter is essential for the gate operation. In this study, we revisited the issue more directly; additional direct evidence of the presence of optically induced couplings was provided based on the transverse relaxation rate $(1/T_2)$ of ^{71}Ga in GaAs measured by spin-echo decay measurements under light illumination, which enabled quantitative analyses on the optically induced couplings.

While performing the measurements, however, we encountered a problem related to the small quadrupolar splitting observed in the ^{71}Ga optical pumping spectra. This is in contrast to the single-peaked spectrum observed in the dark, as expected for the cubic symmetry in the zinc blende structure. As quadrupolar splitting occurs only in the light irradiation may reflect the presence of small lattice distortion in the submicron region near the surface where the nuclear spins are polarized due to the optical pumping effect. In previous experiments, no quadrupolar splitting was observed, neither under light illumination nor in the dark based on a wafer obtained from a different vendor[9,10]. These results indicate that splitting is not inherent in the undoped GaAs crystals[11,12]. Currently, the reason for the splitting has not been resolved. It might be caused by local distortion near some defects or that induced near the free surface. Nevertheless, we do not address the origin of this quadrupolar splitting here, as it is beyond the scope of this study. The problem here is the quadrupolar splitting causes oscillatory behaviors in the spin-echo decay curves[13] that could obscure the decay process. Therefore, in this study, we circumvented this problem by using the envelopes of the decay curves to extract the real spin-echo decay processes from the quadrupolar-modulated spin-echo decays.

[1]National Institute for Materials Science, Tsukuba, Ibaraki 305-0003, Japan. ✉email: GOTO.Atsushi@nims.go.jp

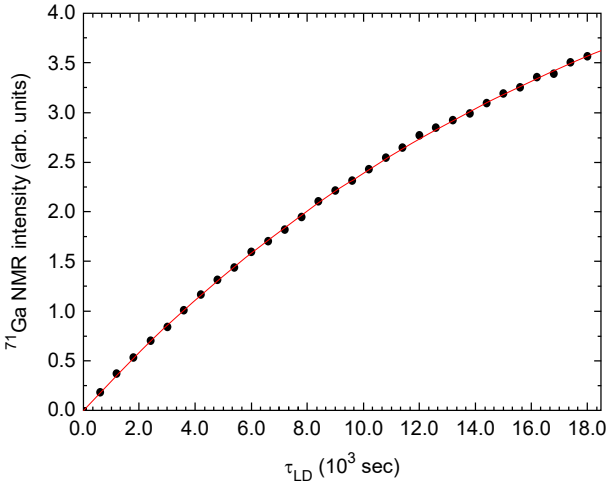

Fig. 1 ^{71}Ga spin lattice relaxation in the dark. Spin lattice relaxation process of the ^{71}Ga nuclei measured with the saturation recovery sequence (Comb pulses -τ_{LD} - $\pi/2$ pulse -FID) at 10 K and in the dark. The horizontal scale, τ_{LD} is the long delay between the saturation pulses and the $\pi/2$ pulse. The solid curve is a fit to the single exponential function.

RESULTS

Single- and double-resonance spin echo experiments in the dark

Let us first consider the process in a dark environment. The spin-echo decay process occurs through a combination of two processes: the so-called T_1 process originating from relaxation during the echo formation and the T_2 process caused by spin–spin couplings. The nuclear magnetization $M(t_1)$ is expressed as[14]

$$M(t_1) = M_0 \exp\left[-\frac{t_1}{T_{2R}} - \frac{1}{2}\left(\frac{t_1}{T_{2G}}\right)^2\right], \quad (1)$$

where M_0 is the initial magnetization, and T_{2R} is Redfield's T_1 process[15], which is the order of T_1. Figure 1 shows the spin–lattice relaxation process of ^{71}Ga measured in the dark. The fitting with a single exponential to the relaxation yields T_1 of 1.9×10^4 s, which is eight orders of magnitude longer than the time scale of the echo decay process (sub-milliseconds). Hence, the T_1 contribution can be safely neglected. Thus, the remaining part is expressed by the Gaussian component represented by T_{2G}. Note that the Gaussian component appears only in the static limit where the spins can be regarded as static during the spin-echo decay process[4–6,15,16], i.e., the nuclear spins other than those manipulated by rf-pulses do not change their states during the pulse sequence. As a spin flip is unlikely to occur when T_1 is long compared to the duration of the sequence, the static limit is apparently fulfilled in the present case. The value of $1/T_{2G}$ includes both direct (nuclear dipolar couplings) and indirect (nuclear spin–spin couplings via electrons) contributions. By neglecting the cross term between them, it can be expressed as $(1/T_{2G})^2 = (1/T_{2G})^2_d + (1/T_{2G})^2_{ind}$ [4–6]. Since no conduction electrons are present in the dark (as apparent from the long T_1), the indirect contribution is negligible; thus, only the direct contribution should be responsible for the decay, i.e., $(1/T_{2G})^2 = (1/T_{2G})^2_d$. The relationship between the direct and indirect contributions to the squared spin echo decay rates is summarized in Table 1.

The sequence used in this study (shown in Fig. 5 in the "Methods" section) is different from that adopted in the usual spin-echo experiments in that an additional flipping pulse for the unobserved nuclei, *S* (P3) is optionally applied concurrently with the second pulse for the observed nuclei, *I* (P2). This is a variation of the spin-echo double resonance (SEDOR) experiments[17,18] and the basis for polarization transfers used as a building block in various two-dimensional NMR schemes[19]. In the present case, the P3 pulse serves as a switch for the heteronuclear spin–spin couplings; if it is on, the *S* nuclei act as 'like-spins' for the *I* nuclei, contributing to the *I*-spin echo decay process. If it is off, the *S* nuclei act as 'unlike spins' for the *I* nuclei and do not affect the *I*-spin echo decay process. Consequently, both the homo- and heteronuclear couplings contribute to the decay in the former—i.e., $(1/T_{2G})^2 = (1/T_{2G})^2_{homo} + (1/T_{2G})^2_{hetero}$—whereas only the homo-nuclear couplings contribute to the decay in the latter — i.e., $(1/T_{2G})^2 = (1/T_{2G})^2_{homo}$. The roles of the P3 pulse are also summarized in Table 1. In the present experiments, the strength of the P3 pulse was adjusted, such that the P2 and P3 pulses featured the same flipping angle by using the Hartmann–Hahn condition in the cross-polarization experiments.

Table 1. Effects of the light illumination and the application of P3 pulse on the homo- and heteronuclear components of the squared spin echo decay rates: $(1/T_{2G})^2_{homo}$ and $(1/T_{2G})^2_{hetero}$.

Light	P3 pulse	Direct coupling		Indirect coupling	
		$(1/T_{2G})^2_{homo}$	$(1/T_{2G})^2_{hetero}$	$(1/T_{2G})^2_{homo}$	$(1/T_{2G})^2_{hetero}$
Off	Off	On	Off	Off	Off
	On	On	On	Off	Off
On	Off	On	Off	On	Off
	On	On	On	On	On

The effect of the P3 pulse is demonstrated through the 2-D contour plots of the echo spectra with and without the P3 pulse measured in the dark, which are shown in Fig. 2a and b, respectively, where the F1 and F2 axes correspond to the Fourier transforms of the indirect (t_1) and direct (t_2) time domains, respectively. The spectra projected onto the F2 axis (the widths correspond to $1/T_2^*$) are similar in the two cases, whereas those projected onto the F1 axis ($1/T_2$) are different from each other due to the effect of the additional P3 pulse, as explained above. That is, both the homo- (^{71}Ga-^{71}Ga) and heteronuclear (^{71}Ga-^{75}As) couplings contribute to the line width in Fig. 2a (P3 on), whereas only the homonuclear spin–spin coupling (^{71}Ga-^{71}Ga) contributes to the line width in Fig. 2b (P3 off).

Figure 3a shows the normalized spin-echo decay curves in the dark, where the triangles and squares represent those measured with and without the P3 pulse, respectively. Here, the intensity at each t_1 point was recorded at the peak of the spectrum obtained by Fourier-transforming the second half of the echo signal, which corresponded to the integral of the echo intensity in the time domain. The decay curves could be well-characterized by Gaussian functions. Fitting the data with Gaussian functions yields the Gaussian rate $1/T_{2G}$ of $6.09 \pm 0.06 \times 10^3$ s^{-1} for P3 on and $4.10 \pm 0.08 \times 10^3$ s^{-1} for P3 off. The difference between the two corresponds to the heteronuclear component associated with $(1/T_{2G})^2_{hetero}$.

Single- and double-resonance spin echo experiments under light illumination

In this section, the experiments under light illumination are discussed. Figure 3b and c shows the normalized spin-echo decay curves with and without the P3 pulse, respectively, under continuous light illumination (σ^+, 826 nm) with two different light powers corresponding to approximately 34 mW and 68 mW at the sample surface with the spot size of approximately φ5 mm, corresponding to the average light intensities of approximately 173 and 346 mW cm^{-2}, respectively. These data were obtained by subtracting the contributions from the dark part of the sample (the data measured under the same conditions but in the dark) from the raw data. As a reference, those measured in the dark (Fig. 3a) are also shown in Fig. 3b and c.

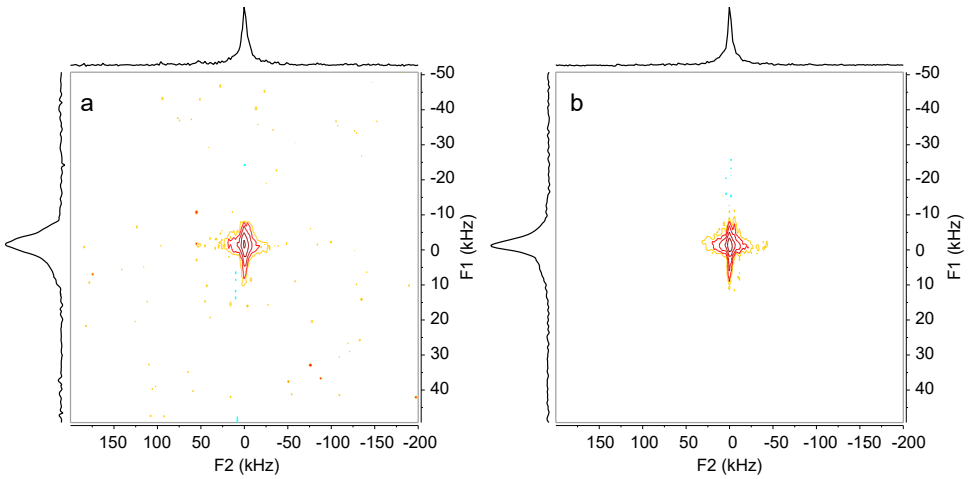

Fig. 2 Single- and double-resonance spin-echo experiments in the dark. Contour plots of the two-dimensional spin-echo experiments with (**a**) and without the *S*-spin flip (P3) pulse (**b**) measured in the dark, with $\tau_L = 20$ min at 10 K. F1 and F2 are the frequencies corresponding to the Fourier transform of the t_1 and t_2 time domains in the SEDOR pulse sequence shown in Fig. 5, respectively. The one-dimensional spectra shown near the F1 and F2 axes are the cross-sections along the F1 and F2 directions that pass the peak intensity, respectively. The spectra projected onto the F2 axis are similar in the two cases, while those projected onto the F1 axis are different from each other due to the effect of the additional P3 pulse. This difference is due to the heteronuclear spin–spin coupling.

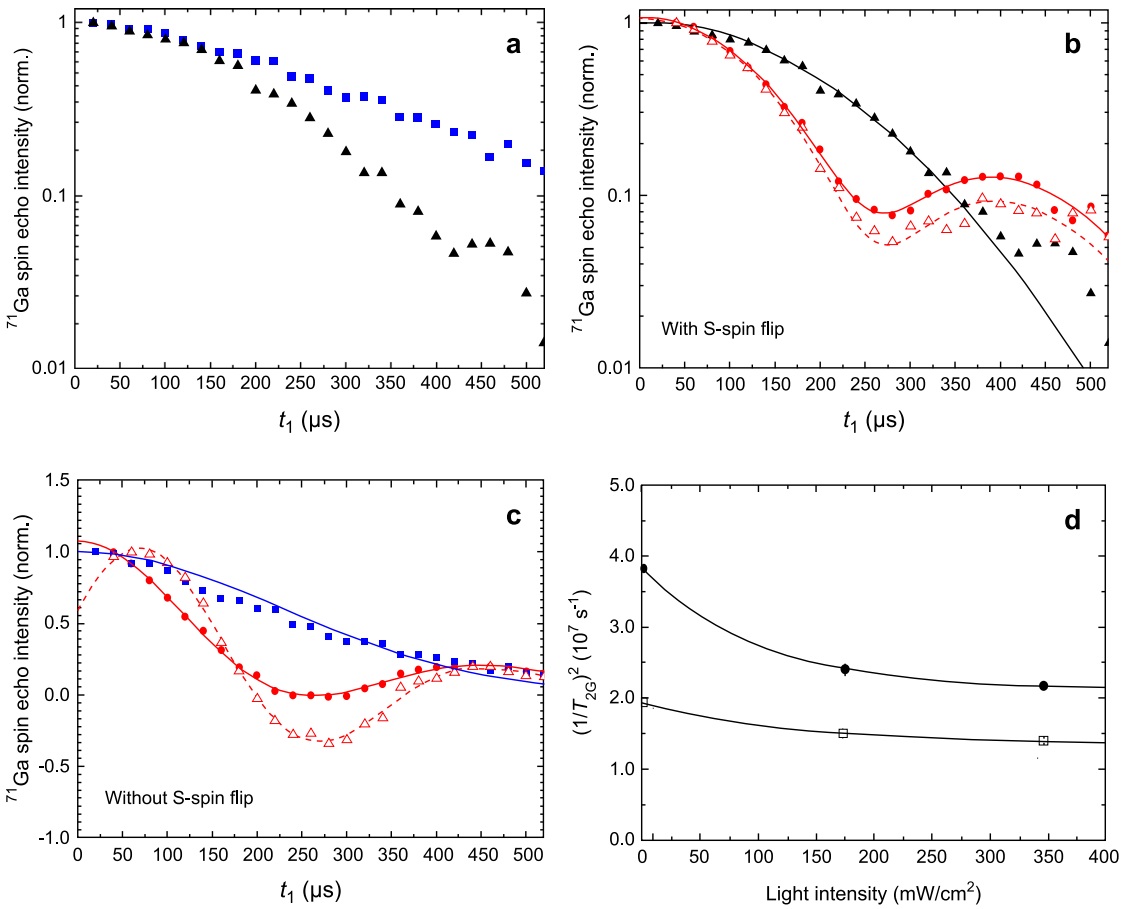

Fig. 3 Single- and double-resonance spin echo experiments under light illumination. a. [Spin echo decay in the dark]: Semi-log plots of the normalized spin-echo decay processes with (▲) and without (■) the *S*-spin flip (P3) pulse measured in the dark, with $\tau_L = 20$ min at 10 K. **b** and **c**. [Spin echo decay under the light illuminations]: Normalized spin-echo decay processes with and without the S-spin flip (P3) pulse, respectively, measured under light illumination with $\tau_L = 5$ min at 10 K, along with the corresponding data in the dark shown in **a**. Solid circles (●) and open triangles (Δ) represent those with the light intensities of approximately 173 and 346 mW cm^{-2}, respectively. The vertical axis in **c** is shown on the linear scale to indicate the negative values in the range 200–340 μs. **d**. [Light intensity dependence of the decay rate]: $(1/T_{2G})^2$ obtained by fitting the data in **b** and **c** with Eq. (2), plotted as a function of the light power. Solid circles (●) and open squares (□) correspond to those with and without the S-spin flip (P3) pulse.

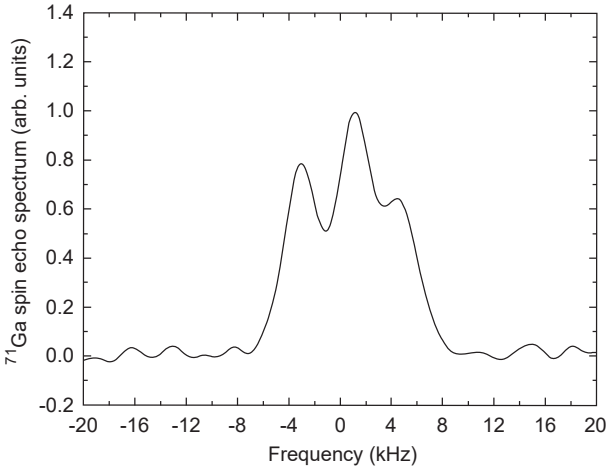

Fig. 4 ^{71}Ga NMR spectrum measured under light illumination. NMR spectrum of the ^{71}Ga nuclei measured under light illumination with an intensity of 346 mW cm^{-2}. In addition to the central transition line, two satellites are observed, and from the interval between them, the nuclear quadrupolar coupling (ν_Q) of approximately 3.8 kHz is determined. The value of ν_Q coincides with twice the inverse of the echo modulation period (530 μs) obtained from the fittings of the modulated decays shown in Fig. 3b and c using Eq. (2), indicating that the echo modulation is caused by the quadrupolar coupling. The imbalance between the two satellites is due to the low nuclear spin temperature caused by the cooling effect of the optical pumping. Note that the ratio of the intensities between the central transition and the two satellites does not reflect the transition probabilities, owing to the different quadrupolar modulations[13].

Before discussing the effects of the P3 pulse, we must first focus on the oscillatory behaviors appearing only under light illumination. This modulation is caused by the effect of the I_z^2 terms in the quadrupolar interaction Hamiltonian on the time development of the density matrix, first indicated by Abe et al.[13]. Here, the oscillatory behaviors should be observed only in single crystals, where the nuclear quadrupolar interaction is well defined, and the modulation period is directly related to the nuclear quadrupolar interaction. That is, the amplitude of the echo signal E is written as a function of t_1 as[13,20],

$$E(t_1) = M(t_1)[C_0 + C_1\cos(at_1 + \delta_1) + \cdots], \quad (2)$$

where C_0, C_1, and δ_1 are the constants depending on the excitation conditions, and a is the oscillation period given by the nuclear quadrupolar frequency: $a = [3e^2qQ/8\hbar\, I(2I-1)](3\cos^2\theta - 1)$, where eq, Q, and I are the electric field gradient (EFG), the nuclear quadrupole moment, and the nuclear spin quantum number, respectively, and θ is the angle between the principal axis of the EFG and the magnetic field. In the present case, $I = 3/2$ for ^{71}Ga and $\theta = 0$; hence, $a = 2\pi(e^2qQ/2h)/2 = 2\pi\nu_Q/2$, where $\nu_Q = e^2qQ/2h$ is the nuclear quadrupolar frequency. That is, the modulation frequency is given by $\nu_Q/2$. In fact, the value of ν_Q obtained in the FT spectrum coincides with the modulation frequency. The FT spectrum of the echo signal under a light intensity of 346 mW cm^{-2} is shown in Fig. 4. Half of the interval between the two satellites yields $\nu_Q = 3.8$ kHz, which coincides with twice the inverse of the echo modulation period (530 μs) obtained from the fittings of the modulated decays to Eq. (2), as shown below.

In contrast to the well-defined modulation period, however, the other three constants (C_0, C_1, and δ_1) are sensitive to the pulse conditions, particularly to the pulse widths[13,20]. Nevertheless, focusing only on the point at which $\cos(at_1 + \delta_1) = 1$, the second term in the square bracket on the right-hand side of Eq. (2) becomes C_1. Hence, ignoring the higher term in the bracket, the decay curves obey $(C_0 + C_1)M(t_1)$, i.e., the decay without quadrupolar modulation. In the present experiments, we set the pulse condition such that the phase shift δ_1 was as close to zero as possible. In this case, the envelope of the decay represents the original $M(t_1)$, which can be directly compared with that in the dark.

In Fig. 3b, where the P3 pulse is on, the normalized intensities under the light illumination are clearly higher than those in the dark at $t_1 \sim 530$ μs, where $\cos(at_1 + \delta_1) = 1$, hence the quadrupolar modulation can be neglected, and the difference is larger as the light power is higher. Furthermore, in Fig. 3c, where the P3 pulse is off, a weak enhancement of the normalized intensity at t_1 ~530 μs is observed upon light illumination. The data in Fig. 3b and c were fitted using Eq. (2) to obtain $1/T_{2G}$. The results are shown as a function of the light power in Fig. 3d. As expected from the observation shown above, the value of $(1/T_{2G})^2$ decreases with increasing light power under the P3 pulse, while its change is small in the absence of the P3 pulse. Recalling that $(1/T_{2G})^2 = (1/T_{2G})^2_{\mathrm{homo}} + (1/T_{2G})^2_{\mathrm{hetero}}$ in the former and $(1/T_{2G})^2 = (1/T_{2G})^2_{\mathrm{homo}}$ in the latter, the present data indicate that $(1/T_{2G})^2_{\mathrm{hetero}}$ changes upon light illumination (refer to Table 1). Note that the nuclear spin diffusion does not affect the conclusion. The spin diffusion proceeds 100 nm in 5–6 min in solids[21], while the SEDOR sequence is completed in submilliseconds, in which the nuclear spins hardly diffuse in this time scale.

DISCUSSION

This result provides evidence that additional heteronuclear coupling arises from light illumination, and its strength depends on the light intensity. The fact that $(1/T_{2G})^2$ decreases with increasing light power indicates that the total heteronuclear coupling decreases. When both indirect and direct (dipole) couplings exist, the total coupling is given by the sum of these couplings and the cross terms between them contribute to $(1/T_{2G})^2$. As the direct couplings always exist, it is concluded that the additional heteronuclear coupling partially cancels the nuclear dipolar couplings, i.e., the signs of these couplings are opposite.

Meanwhile, the change in homonuclear coupling with light power was small. A possible cause for the difference between the two cases is the reach of the coupling, owing to the fact that the distance between a Ga site and its nearest As sites is smaller than that between Ga and its nearest Ga sites. In previous cross-polarization experiments, the second nearest-neighbor heteronuclear coupling was effective when the average light power exceeded 100 mW[9], implying that a much higher light power would cause a considerably distinct change in $(1/T_{2G})^2$. Another possible cause is that the spin–spin coupling may have an oscillating characteristic, as in the case of the Ruderman–Kittel interaction, as the homonuclear coupling is located near the node of the oscillation. In any case, the sum of the contributions from homo- and heteronuclear couplings approaches that from only the homonuclear couplings with increasing light power; thus, the coupling with the first nearest-neighbor ^{75}As is the dominant contribution to $(1/T_{2G})^2$ in this range of light power. With increasing light power, the optically induced couplings increase and eventually surpass the dipolar couplings. For higher-order nearest neighbors, the nuclear dipolar couplings are small; hence, the optically induced coupling is expected to be dominant. This can be confirmed by experiments with a light source having higher power.

In conclusion, we have shown that nuclear spin–spin coupling in GaAs is induced by light illumination, with the photon energy being close to the band gap. The coupling was manifested in the spin-echo decay process of ^{71}Ga under light illumination. Quadrupolar-modulated echo decay curves were observed, and by analyzing the modulated decays, the real decay processes due

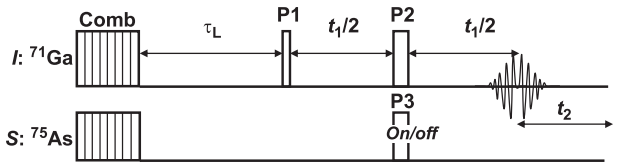

Fig. 5 Pulse sequence for the spin echo experiments. In the beginning, both the *I* (^{71}Ga) and the *S* (^{75}As) nuclear magnetizations are saturated by comb pulses comprised of 32 $\pi/2$-pulses. After the time interval τ_L for the buildup of the nuclear magnetizations, the spin-echo sequence for the *I*-spins is applied (P1 and P2). The *S*-spins are optionally flipped (P3) concurrently with the P2 pulse. An Oldfield echo sequence with the ratio of the P1/P2 pulse widths of 1:2 was used to minimize the distortion of the echo signal due to the quadrupolar effect. The P1/P2 pulse widths were adjusted such that the phase of the echo remains unchanged during the echo decay processes. In the light illumination experiments, the light (826 nm, σ^+) was continuously applied during this sequence.

to the nuclear spin–spin couplings were extracted. The comparison of the decay processes with and without the additional flipping pulse for the ^{75}As nuclei clearly showed that the optically induced couplings increased when light power increased. Moreover, the sign of the induced heteronuclear couplings between Ga–As pairs was opposite to that of the dipolar couplings, canceling each other out. While they are comparable to each other in this range of light power, the optically induced coupling can surpass the nuclear dipolar coupling and become dominant at higher light powers, as demonstrated in the cross-polarization experiments[9].

METHODS

Experimental setup

The sample used in this study was a commercially available semi-insulating undoped GaAs single-crystal wafer with a thickness of 500 μm and crystal orientation of (100). A piece (5 × 10 mm) was cut out of the original 2″ wafer and attached to a sapphire sample stage with grease, and subsequently mounted on an NMR probe as shown below.

The NMR experiments were performed using an optical-pumping double-resonance NMR system operating at cryogenic temperatures[10]. The system features a home-built static NMR probe capable of performing XY double-resonance experiments under light illumination. The probe, with the sample stage at its head, was inserted into a cryostat that was directly connected to a GM cryocooler and installed in a 9.39-T NMR magnet from the bottom. With the probe inserted in the cryostat, the sample stage was thermally contacted to the heat anchor at the bottom of the cryostat, through which the sample was cooled. For the thermal isolation and prevention of arcing, the probe space inside the cryostat was evacuated to less than 10^{-2} Pa. The probe was tuned to *I* (^{71}Ga) and *S* (^{75}As) nuclei, and the sample temperature was set to 10 K.

A continuous-wave diode laser was used to provide the excitation light with a fixed wavelength of 826 nm, around which the maximal optical pumping effect for ^{71}Ga was observed in undoped GaAs[10]. The linearly polarized light emitted from the laser was transmitted to the probe head inside the cryostat through polarization-maintaining optical fibers via the vacuum feedthrough located at the probe base. Subsequently, it was transformed into circularly polarized light by a quarter-wave plate and illuminated the sample normal to the sample surface, i.e., parallel to the magnetic field.

Pulse sequence

The spin-echo pulse sequence used in the experiments is shown in Fig. 5. Following the comb pulses that saturate the initial nuclear magnetizations of both nuclei and a time interval τ_L, a two-pulse sequence was applied, and a spin echo signal was detected. The echo form is sensitive to the pulse conditions, particularly in the presence of quadrupolar couplings. Hence, for the light illumination experiments, we used the sequence with a quadrature phase cycling proposed by the Oldfield group[22,23] and set the ratio of the widths between the first (P1) and the second (P2) pulses at 1:2 to obtain undistorted spectra[22]. The echo signal was recorded as a function of twice the time interval between the two pulses (t_1) to obtain the transverse relaxation time T_2.

DATA AVAILABILITY

The data that support the findings of this study are available from the corresponding author upon reasonable request.

Received: 11 December 2021; Accepted: 22 April 2022;
Published online: 18 May 2022

REFERENCES

1. Ruderman, M. A. & Kittel, C. Indirect exchange coupling of nuclear magnetic moments by conduction electrons. *Phys. Rev.* **96**, 99–102 (1954).
2. Suhl, H. Effective nuclear spin interactions in ferromagnets. *Phys. Rev.* **109**, 606 (1958).
3. Nakamura, T. Indirect coupling of nuclear spins in antiferromagnet with particular reference to MnF_2 at very low temperatures. *Prog. Theor. Phys.* **20**, 542–552 (1958).
4. Pennington, C. H. & Slichter, C. P. Theory of nuclear spin-spin coupling in $YBa_2Cu_3O_{7-\delta}$. *Phys. Rev. Lett.* **66**, 381–384 (1991).
5. Itoh, Y. et al. ^{63}Cu(2) nuclear spin-spin relaxation in $YBa_2Cu_3O_{6.98}$, $YBa_2(^{63}Cu)_3O_{7-\delta}$, and $YBa_2Cu_4O_8$. *J. Phys. Soc. Jpn.* **61**, 1287–1298 (1992).
6. Pennington, C. H. & Slichter, C. P. In *Physical properties of high temperature superconductors* (ed. Ginsberg, D. M.) (Singapore: World Scientific, 1991).
7. Kane, B. E. A silicon-based nuclear spin quantum computer. *Nature* **393**, 133–137 (1998).
8. Goto, A., Shimizu, T., Hashi, K., Kitazawa, H. & Ohki, S. Decoupling-free NMR quantum computer on a quantum spin chain. *Phys. Rev. A* **67**, 022312 (2003).
9. Goto, A., Ohki, S., Hashi, K. & Shimizu, T. Optical switching of nuclear spin–spin couplings in semiconductors. *Nat. Commun.* **2**, 378 (2011).
10. Goto, A., Ohki, S., Hashi, K. & Shimizu, T. Optical-pumping double-nuclear-magnetic-resonance system with a Gifford–McMahon cryocooler. *Jpn. J. Appl. Phys.* **50**, 126701 (2011).
11. Paravastu, A. K. & Reimer, J. A. Nuclear spin temperature and magnetization transport in laser-enhanced NMR of bulk GaAs. *Phys. Rev. B* **71**, 045215 (2005).
12. Hayes, S. E., Mui, S. & Ramaswamy, K. Optically pumped nuclear magnetic resonance of semiconductors. *J. Chem. Phys.* **128**, 052203 (2008).
13. Abe, H., Yasuoka, H. & Hirai, A. Spin echo modulation caused by the quadrupole interaction and multiple spin echoes. *J. Phys. Soc. Jpn.* **21**, 77–89 (1966).
14. Abragam, A. *The principles of nuclear magnetism* (Oxford: Oxford University Press, 1961).
15. Redfield, A. G. The Theory of relaxation processes. *Adv. Magn. Reson.* **1**, 1–32 (1965).
16. Goto, A. et al. Origin of the enhanced copper spin echo decay rate in the pseudogap regime of the multilayer high-T_c cuprates. *Phys. Rev. Lett.* **89**, 127002 (2002).
17. Kaplan, D. E. & Hahn, E. L. Expériences de double irradiation en résonance magnétique par la méthode d'impulsions. *J. Phys. Radium* **19**, 821–825 (1958).
18. Emshwiller, M., Hahn, E. L. & Kaplan, D. Pulsed nuclear resonance spectroscopy. *Phys. Rev.* **118**, 414–424 (1960).
19. Ernst, R. R., Bodenhausen, G. & Wokaun, A. *Principles of nuclear magnetic resonance in one and two dimensions* (Oxford: Oxford University Press, 1987).
20. Brener, R. & Ehrenfreund, E. Quadrupole interaction measurements in some $CsBX_3$ (B=Ni, Mg; X=Cl, Br) crystals by spin-echo modulation. *J. Magn. Reson.* **26**, 539–541 (1977).
21. Ramanathan, C. Dynamic nuclear polarization and spin diffusion in non-conducting solids. *Appl. Magn. Reson.* **34**, 409–421 (2008).
22. Kunwar, A. C., Turner, G. L. & Oldfield, E. Solid-state spin-echo Fourier transform NMR of ^{39}K and ^{67}Zn salts at high field. *J. Magn. Reson.* **69**, 124–127 (1986).
23. MacKenzie, K. J. D. & Smith, M. E. Multinuclear solid-state NMR of inorganic materials, (Pergamon Materials Series, Pergamon, Amsterdam, 2002), Vol. 6, Section 3 **4**, 133.

ACKNOWLEDGEMENTS

We appreciate the technical assistance provided by the staff of the NMR station of NIMS. This work was partially supported by JSPS KAKENHI (Grant Number 21K18897).

AUTHOR CONTRIBUTIONS

A.G. conceived and designed the experiments. All the authors jointly designed the system for the experiments, and A.G. and S.O. constructed it. A.G. carried out the main experiments. All the authors were involved in the analyses. A.G. wrote the paper with the help of the co-authors.

COMPETING INTERESTS

The authors declare no competing interests.

ADDITIONAL INFORMATION

Correspondence and requests for materials should be addressed to Atsushi Goto.

Reprints and permission information is available at http://www.nature.com/reprints

Publisher's note Springer Nature remains neutral with regard to jurisdictional claims in published maps and institutional affiliations.